北京正负电子对撞机国家实验室

# 2001

# 北京同步辐射装置用户科技论文集

（下册）



北京正负电子对撞机国家实验室办公室编印

# 序

2000-2001 运行年度，BSRF 的工作一直得到广大用户的极大支持和关爱，使我们的工作又有长足的进展。同步辐射专用运行机时增加，光源质量进一步改善，课题管理更加完善，研究领域有所扩展，研究水平不断提高。经过多年的积累，许多研究课题取得了丰硕的成果，有的课题取得了重大突破，一些具有创新性、高难度的课题也取得了不同程度的进展。

为了促进 BSRF 与国内、外科学家的交流合作，也作为 BSRF 工作的鞭策。我们从 1997 年起收集用户和 BSRF 工作人员在 BSRF 上全部或部分实验发表的论文。每年编辑一册 "北京同步辐射装置上的科学研究论文集"。 2001 年在国内外学术杂志上发表论文 131 篇(不完全统计)，本论文集共收集用户论文 102 篇，其中 SCI 收录 110 余 篇，影响因子 1—1.5 的 19 篇，1.5—2.0 的 10 篇，大于 2 的 8 篇。本论文集是 2000-2001 运行年度 BSRF 科研工作的缩影，是广大用户和 BSRF 工作人员辛勤劳动和聪明才智的结晶。在此，我们感谢为 BSRF 发展做出贡献的广大用户和 BSRF 工作人员。由于各种原因，可能还有一些高水平的论文没有收集到 "论文集" 中，我们谨向这些论文的作者表示深深的歉意。

另有部分文章已在“高能物理与核物理”2001 年增刊刊载，为了避免重复，本文集只登录文章目录，原文请见高能物理与核物理(GAONENG WULI YU HEWULI) 第 25 卷 增刊。

2001 年 4 月

# 北京同步辐射装置用户 2001 年科技论文目录

## (下　册)

### 【小角散射实验站】



### 【衍射实验站】



### 【LIGA、光刻实验站】



### 【形貌学实验站】

## 【高压衍射实验站】



## 【漫散射实验站】



## 【软 X 实验站】



## 【其他】

# Effect of Gas Antisolvent on Conformation of Polystyrene in Toluene: Viscosity and Small-Angle X-ray Scattering Study

**Dan Li, Buxing Han,* Zhimin Liu, Jun Liu, Xiaogang Zhang, Shougang Wang, and Xifeng Zhang**

*Center for Molecular Sciences, Institute of Chemistry, Chinese Academy of Science, Beijing 100080, China*

**Jun Wang and Baozhong Dong**

*Institute of High Energy Physics, Chinese Academy of Science, Beijing 100039, China*

*Received August 16, 2000; Revised Manuscript Received January 15, 2001*

ABSTRACT: Synchrotron radiation small-angle X-ray scattering (SAXS) and the viscosity technique were used to investigate the effect of dissolved $CO_2$ in toluene on the conformation of polystyrene (PS) in the solution. The viscosity of PS solution decreases faster with increasing antisolvent $CO_2$ pressure than that of the solvent in the absence of the polymer. The intrinsic viscosity $[\eta]$ calculated using the well-known Huggins equation decreases with antisolvent pressure. It was found that the second virial coefficient $A_2$ and the apparent mean-square radius of gyration $\langle R_g^2\rangle^{1/2}$ decreases with pressure of antisolvent $CO_2$. All these phenomena can be attributed to the shrink of PS chain in the course of adding the gas antisolvent because the interaction between the polymer and solvent becomes weaker. The values $\langle R_g^2\rangle^{1/2}$ at different pressures obtained from SAXS data agree reasonably with those calculated from Flory theory using the viscosity data determined in this work. This implies that Flory theory, which has been used widely for the solutions of polymers in liquid solvents, is also applicable to the polymer solution with gas antisolvent.

## Introduction

Compressed fluids, including supercritical fluids, have been used in polymer separation and purification processes such as extraction and fractionation,[1] impregnation of polymers with additives, and conditioning polymer films.[2,3] Recently, several innovative processes have been developed which utilize compressed fluids in the production of advanced polymeric materials such as microcellular foams, gels, fibers, and particles.[4,5] $CO_2$ is a desirable solvent for polymer processing since it is nontoxic, nonflammable, and inexpensive. After processing, $CO_2$ can be removed from the polymers completely simply by decreasing the pressure.

The use of compressed $CO_2$ for fine particle formation is a rapidly developing field of research.[1] The gaseous antisolvent (GAS) process is one of the most important ones.[6] The possibility of obtaining solvent free microparticles with narrow size distribution makes this technology especially attractive. The basis of GAS technique[7] is that a dense gas is generally soluble in organic solvents and in solutions with the solutes. Dissolution of gas causes a volume expansion of the solvent and lowers solvent power, which forces the solute to precipitate. Because of the high and uniform degree of supersaturation, small particles with a narrow size distribution can be obtained. Moreover, it is possible to extract all the solvent in the products, and to obtain solvent-free product. To date, GAS processes have been successfully used in the recrystallization of organic solids,[8,9] the fractionation of natural products,[10,11] the preparation of ultrafine particles et al.[7,12−22] Since only a few kinds of polymers have been found to be soluble in compressed $CO_2$,[23] compressed $CO_2$ can also be used as an environmentally benign antisolvent for processing most polymers. Some related papers have been published,[15−22] and they were mainly focused on how the operating parameters affect the properties of the products. We are very interested in the polymer conformation in GAS process, since the solubility of a gas in an organic solvent can be tuned by pressure and temperature, accordingly, the polymer morphology be tailored. The investigation to this problem has both practical and theoretical importance.

It is well-known that small-angle X-ray scattering (SAXS) and viscosity measurement are useful techniques for studying polymer solutions. In one hand, SAXS can provide information about apparent mean-square radius of gyration $\langle R_g^2\rangle^{1/2}$ and the second virial coefficient ($A_2$), which are related to the conformation of the polymer and intermolecular interaction in the solution, respectively.[24] Some papers have been published for studying polymer solutions by SAXS in the absence of gas antisolvent.[25−30] On the other hand, evaluation of intrinsic viscosity, $[\eta]$, can provide valuable information on the changes in the solvent−polymer interactions as the system conditions are changed. An important quantification of this relationship is given by the dilute solution theory of Flory,[31] which shows that $[\eta]$ at a given molecular weight is dependent on $\langle R_g^2\rangle^{1/2}$. The effects of temperature, pressure, solvent quality, concentration, chain architecture, and molecular weight upon both $\langle R_g^2\rangle^{1/2}$ and $[\eta]$ have been explored by extensive theoretical efforts and many experimental studies.[32−36] There have also been a number of previous high-pressure studies on polymer solutions in the absence of gas antisolvent, which involve $[\eta]$, $\langle R_g^2\rangle^{1/2}$, ($A_2$), and hydrodynamic radius ($R_h$).[37−41] Generally, viscosity of a polymer solution increases with hydrostatic pressure (typically ≈ 20% per kbar).[37−40] The radius of gyration, however, shows no consistence trend with pressure,[41] and it may either increase or decrease

* To whom correspondence should be addressed. E-mail: Hanbx@pplas.icas.ac.cn. Telephone: (8610)-62562821. Fax: (8610)-62559373.

10.1021/ma0014463 CCC: $20.00 
Published on Web 03/02/2001

with increasing pressure in good solvent. One of the most important and straightforward relationship was between $\langle R_g^2\rangle^{1/2}$ and $[\eta]$ as given by the theory of Flory:[31]

$$[\eta] = \phi'\langle R_g^2\rangle^{3/2} M^{-1} \quad (1)$$

Here $\phi' = 6^{3/2}\phi \approx 3.7 \times 10^{22}$ dL/mol·cm$^3$, $\phi$ is the Flory constant, $\langle R_g^2\rangle^{1/2}$ is the radius of gyration, and $M$ is the molecular weight.

In this work, SAXS and the viscosity technique were used to study the conformation of polystyrene (PS) chain in PS−toluene solution in the presence of antisolvent $CO_2$. No quantitative study for the effect of a gas antisolvent pressure on the conformation of polymers in solutions was found in a literature survey.

## Experimental Section

**Materials.** The polystyrene (PS) ($M_w = 7.8 \times 10^4$) with narrow molecular weight distribution of 1.1 was kindly supplied by State Key Laboratory of Polymer Science, Institute of Chemistry, Chinese Academy of Sciences. Toluene (AR grade) was produced by Beijing Chemical Factory. The PS/toluene solutions were prepared by the gravimetric method. The original concentrations $C_0$ ($CO_2$-free) in our study were $4.6 \times 10^{-4}$, $6.9 \times 10^{-4}$, $1.07 \times 10^{-3}$, $3.2 \times 10^{-3}$, and $9.2 \times 10^{-3}$ g/cm$^3$.

**Apparatus and Procedures for Volume Expansion and Cloud Point Pressures.** The apparatus consisted mainly of a 30-mL optical stainless steel cell, a magnetic stirrer, a constant temperature water bath, a pressure gauge, a gas cylinder, and a high-pressure pump. The accuracy of the pressure gauge, which was composed of a transducer (FOXBORO/ICT) and an indicator, was ±0.025 MPa in the pressure range 0−20 MPa. The temperature of the water bath was controlled by a HAAKE F3 controller. The temperature was determined using a platinum resistance thermometer (Beijing Chaoyang Automatic Instrument Factory, XMT) with an accuracy of ±0.1 K.

In a typical experiment, a suitable amount of PS/toluene solution was loaded into the optical cell, and the cell was stabilized at the desired temperature. $CO_2$ was charged into the cell using the high-pressure pump until suitable pressure was reached. The stirrer was started. At the beginning, the pressure decreased and the volume of the liquid increased with time because of the dissolution of $CO_2$. The pressure remained constant with time when equilibrium was reached. The volume at equilibrium condition was known by reading the graduations on the cell. Some polymer molecules precipitated when the equilibrium pressure was high enough, which could be seen clearly through the windows of the optical cell. The cloud pressure, which was defined as the pressure at which polymer begins to precipitate, was determined.

**Viscosity and Density Measurements.** The high-pressure apparatus for determining the viscosity and density of the solution saturated with $CO_2$ is shown in Figure 1, which was similar to that used previously.[42] The main difference was that there was a falling slug viscometer[43] between the view cell and the liquid sample bomb, so the viscosity of the solution could be determined at any antisolvent pressures. The viscosity was calculated using the following well-known equation:

$$\eta = k(\rho_s - \rho)t \quad (2)$$

$\eta$ is the viscosity of the solution; $t$ denotes the falling time of slug; $\rho_s$ and $\rho$ stand for the densities of the slug and solution; $k$ is the instrument constant. The viscometer was calibrated using 60, 40, and 20 wt % glycol in water and ethanol at 35 °C. $k$ was determined from the slope of the plot of $\eta$ vs $(\rho_s - \rho)t$.

In a typical experiment, a suitable amount of PS/toluene solution was charged into the optical cell and the viscometer

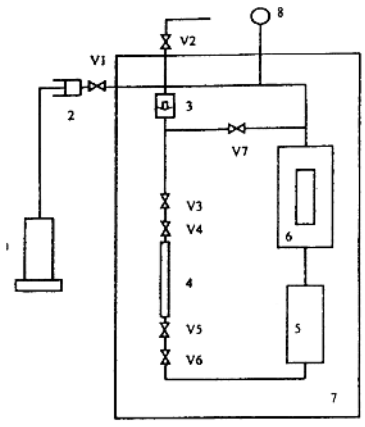


**Figure 1.** Schematic diagram of the experimental apparatus for measuring solubility of $CO_2$ in toluene, and viscosity and density of the liquid phase. Key: (1) gas cylinder; (2) high-pressure pump; (3) solenoid circulation pump; (4) liquid sample bomb; (5) falling slug viscometer; (6) optical cell; (7) constant-temperature bath; (8) pressure gauge, V1−V7 valves.

by vacuum. After the system had reached thermal equilibrium, $CO_2$ was compressed into the system until desired pressure was reached. The solenoid-operated circulation pump was started to circulate the vapor phase through the viscometer, the cell, and the liquid sample bomb. We measured the fall time of the slug about every 30 min, and the circulation pump was stopped during the measurements. The equilibrium was reached when the fall time of the slug did not change with time. The fall time was measured 10−15 times for each equilibrium conditions, and the reproducibility was better than ±0.5%. The density of the solution at each condition was easily known by the volume and mass of liquid sample bomb. The amount of $CO_2$ in the liquid sample bomb was determined by the $PVT$ method.[44] The liquid composition was calculated on the basis of total weight of the liquid sample and the weight of $CO_2$ in the sample.

**SAXS Experiments.** The experimental apparatus for the SAXS study was similar to that used for on-line FT-IR measurement that was described in detail previously.[45] Briefly, the apparatus was consisted mainly of a gas cylinder, a high-pressure pump, a digital pressure gauge, a high-pressure SAXS cell, a thermometer, a temperature controller, and valves and fittings of different kinds. The pressure gauge as described above, consisted of a transducer (FOXBORO/ICT) and an indicator. The schematic diagram of the temperature-controlled SAXS cell is shown in Figure 2. It was composed mainly of a stainless steel body and two diamond windows of 8 mm in diameter and 0.4 mm in thickness. Diamond is an excellent window material for SAXS studies because it has low absorbance and low scattering power. The cell body was coiled with an electric heater and heat-insulate ribbon outside, which is not shown in Figure 2. The X-ray path length of the cell was 1.5 mm, and the internal volume of the cell was 2.7 cm$^3$. There was a small magnetic stirrer in the cell to stir the fluids before the SAXS measurements, so that the equilibrium could be reached in a shorter period of time. The insulated cell was electrically heated to ±0.1 K of the desired temperature by using a temperature controller with a platinum resistance temperature probe (model XMT, produced by Beijing Chaoyang Automatic Instrument Factory).

SAXS experiments were carried out at Beamline 4B9A at the Beijing Synchrotron Radiation Facility, using a SAXS apparatus constructed at the station. A detailed description of the spectrometer was given elsewhere.[46] The detector can

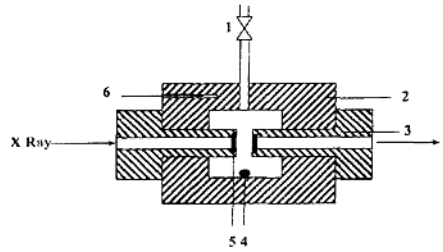


Figure 2. Schematic diagram of the SAXS cell. Key: (1) ball valve; (2) stainless steel body; (3) nut; (4) stirrer; (5) diamond window; (6) thermometer probe.

be translated along the vertical and horizontal axes in a range of 30 mm with a precision of 10 μm. The experiments had an angular resolution of better than 0.5 mrad with this setting. The data accumulation time was 3 min. The angular range was chosen so as to provide data from $h = 0.005$ Å$^{-1}$ to $h = 0.15$ Å$^{-1}$, where the magnitude of scattering vector $h = 2\pi(\sin\theta)/\lambda$, with $\theta$ and $\lambda$ being respectively the scattering angle and incident X-ray wavelength of 1.54 Å. The distance between the sample chamber and the detector was 1.52 m. Background scattering from the slit collimator, the solvent, and the residual air path between the vacuum chamber and the detector was measured and subtracted. It should be mentioned that, for each measurement, the solvent with antisolvent $CO_2$ at the same temperature and pressure was used as the background solvent, so that we could obtain the information on polymer chain. Excess SAXS scattering from the PS solute was also corrected for incident beam decay and transmission.

Before the experiment, SAXS cell was flushed with $CO_2$, and then suitable amount of PS/toluene solution was filled into the cell. $CO_2$ was charged into the cell with stirring at the temperature of interesting. The cell was connected to the SAXS apparatus after the equilibrium was reached and the X-ray scattering was recorded. Moreover, the pressures investigated were the same as those for viscosity study.

**SAXS Data Processing.** We are interested in the conformation of polymer chain in solution in the presence of the antisolvent. Its scattering curve is obtained by subtracting the scattering of the solvent + antisolvent (background scattering) from the scattering of the polymer + solvent + antisolvent solution.

The scattering intensities $I_{exp}(h,C)$ measured as a function of momentum transfer $h$ and polymer concentration $C$ of the polymer, usually expressed in g/cm$^3$, may be treated according to Zimm and Flory and Bouche[24]

$$\frac{KC}{I_{exp}(h,C)} = \frac{1}{M_w I_n(h)} + 2A_2 Q(h) C + \ldots \quad (3)$$

where $K$ is the optical constant, $A_2$ is the second virial coefficient, $M_w$ is molecular weight of the dissolved polymer, and $I_n(h)$ is the single particle scattering function. $Q(h)$ and $I_n(h)$ are normalized in such a way that $I_n(0) = 1$ and $Q(0) = 1$. The first term in right side of eq 3 is merely due to intramolecular interference, whereas the higher term reflect the influence of the intermolecular interference.

From eq 3, if $h \to 0$, we can also obtain the equation[24]

$$\lim_{h\to 0} \frac{KC}{I_{exp}(h,C)} = \frac{1}{M_w}(1 + 2A_2 M_w C + \ldots) \quad (4)$$

from which the thermodynamic analysis of the dilute system can be performed. If $C \to 0$, we can obtain the equation[24]

$$\lim_{c\to 0} \frac{KC}{I_{exp}(h,C)} = \frac{1}{M_w I_n(h)} = \frac{1}{M_w}\left(1 + \frac{\langle R_g^2\rangle}{3} h^2 \ldots\right) \quad (5)$$

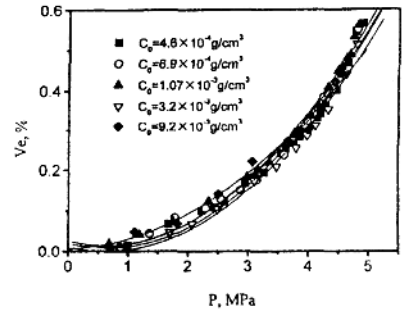


Figure 3. Dependence of volume expansion of the solutions with different original PS concentrations ($C_0$) on antisolvent $CO_2$ pressure.

which contains all information on the shape and the conformation of the isolated macromolecules in solution. The initial slopes of eq 4 vs $C$ and eq 5 vs $h^2$ yield the second virial constant $A_2$ and mean square radius of gyration $\langle R_g^2\rangle^{1/2}$, respectively. The $K$ is required to use eqs 4 and 5. To a first approximation, we only consider the first two terms of the right side in eq 3. At the angle of $h = 0$, from eq 3, we have

$$\frac{KC}{I_{exp}(0,C)} = \frac{1}{M_w} + 2A_2 C \quad (6)$$

or

$$\frac{1}{M_w C} = -2A_2 + \frac{K}{I_{exp}(0,C)} \quad (7)$$

Thus, K and $A_2$ can be obtained from the slope and intercept of the $1/M_wC$ vs $1/I_{exp}(0,C)$ plot.

## Results and Discussion

**1. Phase Behavior.** The volume expansion $V_e$ and cloud pressure of the solutions were determined at different antisolvent pressures in the temperature range from 298.15 to 328.15 K. In this work, $V_e$ is defined as $(V - V_0)/V_0$, where $V$ and $V_0$ are the volumes of the solution after and before dissolving $CO_2$. As examples, Figure 3 shows the $V_e$ data of the solutions of different original concentrations at 308.15 K and different pressures. The $C_0$ in the figure is the original concentration of PS ($CO_2$-free). The $V_e$ experiments were repeated at least three times for each equilibrium condition and the reproducibility was better than ±1%. It was estimated that the accuracy of the measurements was better than ±2%. Figure 3 shows that the effect of PS concentration on the $V_e$ is very limited. Figure 4 shows the cloud point pressures of the solutions of various original concentrations at different temperatures. As expected, the cloud pressure decreases with the original concentration of PS. Obviously, the concentration of a solution decreases with $V_e$ or pressure. The $V_e$ and cloud point pressure data in Figures 3 and 4 allowed us to determine how much $CO_2$-free solution should be charged into the SAXS cell at different temperatures and pressures and what conditions we should choose for the viscosity and SAXS investigations.

The solubility of $CO_2$ in the solution is directly related with pressure. The solubility of $CO_2$ and the densities of the solutions of different PS concentrations were determined at 308.15 K and different antisolvent pres-

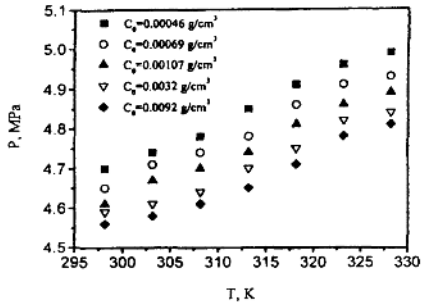


**Figure 4.** Cloud point pressures of solutions with different original PS concentrations ($C_0$) at different temperatures.

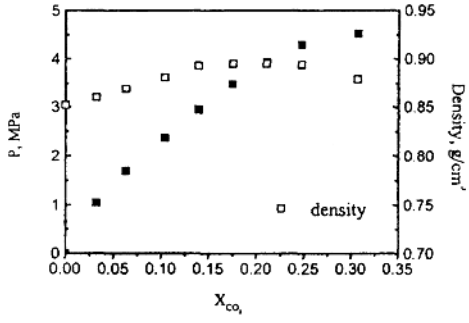


**Figure 5.** Effect of pressure on the solubility of $CO_2$ in toluene $X_{CO_2}$ (weight fraction) and the density of the liquid phase at 308.15 K ($C_0$ = 0.00046 g/cm³).

sures. As an example, Figure 5 shows the solubility of $CO_2$, $X_{CO_2}$ (weight fraction), in an PS/toluene solution ($C_0$ = 0.00046 g/cm³) as a function of its partial pressure at 308.15 K. As expected, the solubility increases with its partial pressure. The corresponding density of the liquid phases is also shown in the figure, which was required in the viscosity calculation as can be known from eq 2. It should be mentioned that the effect of $C_0$ on the solubility and density is not noticeable at our experimental conditions. By combination of the results in Figures 3 and 5, the pressure–volume expansion-composition relation can be known.

**2. Viscosity.** In this work, we determined the viscosity $\eta$ of PS/toluene solutions with original concentrations of $4.6 \times 10^{-4}$, $6.9 \times 10^{-4}$, $1.07 \times 10^{-3}$, $3.2 \times 10^{-3}$, and $9.2 \times 10^{-3}$ g/cm³. The pressure of antisolvent $CO_2$ was up to 4.2 MPa. The results at 308.15 K are shown in Figure 6. It should be emphasized that all the experiments were conducted under equilibrium conditions.

The results in Figure 6 show that $\eta$ decreases linearly with pressure of $CO_2$ at fixed temperature. The main reason is because the dissolved $CO_2$ can reduce viscosity of a liquid. It is also interesting to notice that the decrease in viscosity with pressure is greater for the concentrated solutions than in dilute solutions; i.e., $\eta$ is more sensitive to pressure for concentrated solutions. This must be related with conformation change of the polymer in solvent, which results from weaker interaction between the polymer and the solvent with adding antisolvent $CO_2$.

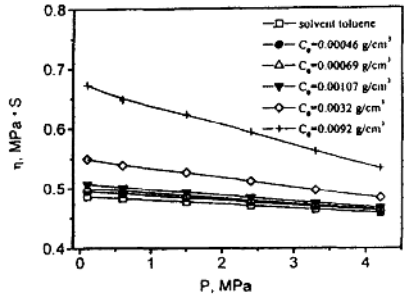


**Figure 6.** Dependence of the viscosity of the solutions $\eta$ on antisolvent $CO_2$ pressure at 308.15 K for different original concentrations ($C_0$).

To understand the effect of antisolvent pressure upon the configuration of the dissolved polymer, we calculate the specific viscosity as a function of pressure

$$\eta_{sp} = \eta(p)/\eta_0(p) - 1 \tag{8}$$

where $\eta_{sp}(p)$ is specific viscosity at constant pressure, $\eta(p)$ and $\eta_0(p)$ are viscosity of the solution and solvent at the same pressure, respectively. This ratio effectively removes the solvent-dominated viscosity and allows for a direct examination of polymer behavior. This is also the first step to obtain the intrinsic viscosity[47] from which dilute solution polymer theory can be applied

$$[\eta] = \lim_{c \to 0}(\eta_{sp}/C(p)) \tag{9}$$

where $[\eta]$ is intrinsic viscosity, and $C(p)$ is the concentration of the solution at different antisolvent pressure which can be easily calculated from original PS concentration and the volume expansion shown in Figure 3.

$[\eta]$ is calculated from $\eta_{sp}$ by the familiar Huggins equation[47]

$$\frac{\eta_{sp}(p)}{C(p)} = [\eta] + k_H[\eta]^2 C(p) + \ldots \tag{10}$$

where $K_H$ is the Huggins interaction parameter which is related to the shape of the polymer molecules and its degree of association.

$\eta_{sp}(p)/C(p)$ is plotted against the concentration at different pressures $C(p)$ in Figure 7. Intrinsic viscosity $[\eta]$ and Huggins constants can be obtained from the intercepts and the slopes of the curves, respectively. The results are listed in Table 1. As shown in Table 1, the intrinsic viscosity $[\eta]$ decreases with pressure. The intrinsic viscosity is directly related with the conformation of the polymer in the solution and it is higher when the polymer is extended. It is also well-known that a polymer chain is more extend in good solvent. In our experimental system, toluene is a good solvent for PS, while $CO_2$ is a very poor and used as an antisolvent. The solvent power of toluene is reduced in the course of adding antisolvent $CO_2$, since the solubility of $CO_2$ in the solvent increases with pressure; i.e., the solvent strength decreases with pressure. Thus, it is not surprised that the intrinsic viscosity is highest in toluene, and decreases with the partial pressure of $CO_2$.

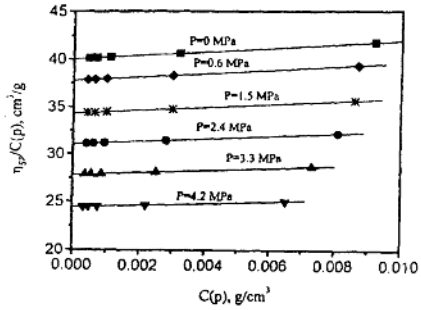


**Figure 7.** Huggins plots for PS in toluene at different antisolvent $CO_2$ pressures.

**Table 1. Intrinsic Viscosity and Huggins Constant under Different Pressures of Antisolvent $CO_2$ for Polystyrene in Toluene at 35 °C**

| pressure, MPa | $[\eta]$, cm³/g | Huggins const | overlap concn $C^*$, g/cm³ |
|---|---|---|---|
| 0 | 40.02 | 0.120 | 0.154 |
| 0.6 | 37.79 | 0.125 | 0.163 |
| 1.5 | 34.32 | 0.132 | 0.179 |
| 2.4 | 31.04 | 0.140 | 0.198 |
| 3.3 | 27.79 | 0.148 | 0.221 |
| 4.2 | 24.42 | 0.155 | 0.252 |

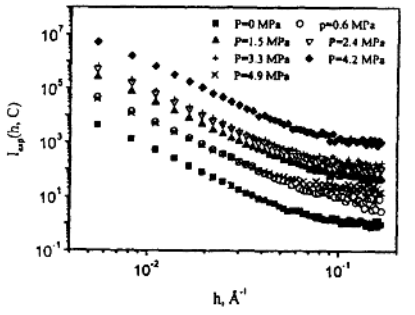


**Figure 8.** Effect of antisolvent $CO_2$ pressure on SAXS spectra of the solution ($C_0$ = 0.00046 g/cm³).

The overlap concentration $C^*$ at which polymer coils begin to overlap and entangle can be calculated from[48,49]

$$C^* = M/(N_A R_g^3) \qquad (11)$$

where M and $R_g$ are molecular weight and gyration radius of a polymer chain respectively, and $N_A$ is Avogadro's number. The radius of gyration was calculated from intrinsic viscosity data in Table 1 and Flory solution theory[31] as described in eq 1. The results showed that the concentrations of the solutions studied in this work were much lower than overlap concentration, i.e., the polymers in the solutions were not overlapped.

**3. SAXS Study.** In this work, we determined scattering intensity at original PS concentrations of 4.6 × $10^{-4}$, 6.9 × $10^{-4}$, 1.07 × $10^{-3}$, 3.2 × $10^{-3}$, and 9.2 × $10^{-3}$ g/cm³ at the same antisolvent pressures as those for viscosity measurements. As examples, Figure 8 shows double logarithm plot of scattering intensity $I_{exp}(h,C)$ vs scattering angle h at $C_0$ = 4.6 × $10^{-4}$ g/cm³ and different antisolvent $CO_2$ pressures, with $I_{exp}(h,C)$ being the scattered intensity due to the PS solute.

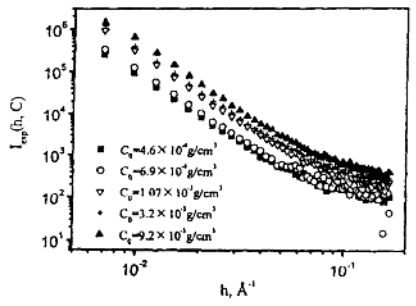


**Figure 9.** Effect of original solution concentration ($C_0$) on SAXS spectra of the solutions at antisolvent $CO_2$ pressure of 2.40 MPa.

The scattering intensity increases with pressure at pressures lower than cloud pressure. We have known that the X-ray scattering is due to the contrast provided by the difference in electron densities in the solute and solvent. In the system investigated here, the electron density of the solute PS is 0.343 e/Å³ and that of the solvent toluene is 0.282 e/Å³.[50] The increasing of the scattering intensity may result from the aggregation of the polymer chain. Another feature of SAXS profiles is that the scattering intensity at the pressure higher than cloud pressure decreases considerably. It may result from the precipitation of some PS in the solution because the pressure is higher than the cloud pressure. The precipitated PS dropped below the irradiated volume.

Figure 9 shows double logarithm plot of $I_{exp}(h,C)$ vs $h$ for PS/toluene solutions of different original concentrations at 2.4 MPa. The magnitude of the polymer concentration effect depends on the shape and charge of the particle and the solvent. No general function exists which would allow prediction of the magnitude of the concentration effect. From Figure 9, we can say that the concentration has a large effect on the scattering of the polymer solution.

To use eq 7 to obtain $A_2$ and $K$ at different antisolvent pressures, the double logarithm scattering intensity plots of $I_{exp}(h,C)$ vs h at different concentrations were obtained using the experimental data. The concentration $C$ has been corrected for the volume expansion using the results in Figure 3. The data were extrapolated to $h = 0$, and the values of $I_{exp}(0,C)$ were obtained. Figure 10 shows the $1/M_w$C vs $I_{exp}(0,C)$ curves which are linear in the concentration range studied in this work. This verifies that we can get reliable results although we only considered the first two terms in the right side of eq 3. Thus, $K$ and $A_2$ at different antisolvent pressures were easily obtained from slope and intercept of $1/M_w$C vs $I_{exp}(0,C)$ curves, and the results are listed in Table 2.

We could not find the $A_2$ data in the presence of gas antisolvent in the literature. However, the $A_2$ of the PS–toluene binary solution reported by Berry et al.[51] was 0.00055, which was close to that obtained in this work.

The second virial constant $A_2$ is related with the solvent power of the solvent for the polymer. As expected, $A_2$ depends on the partial pressure of antisolvent

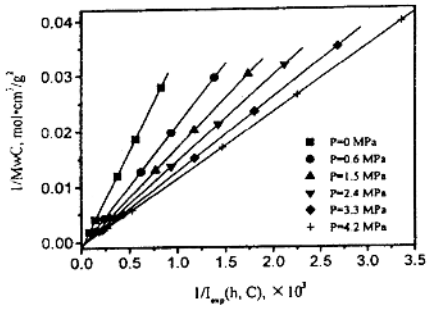


**Figure 10.** Plots of $1/M_wC$ against $1/I_{exp}(0,C)$ at different antisolvent pressures.

**Table 2. Values of $K$, $A_2$, and $\langle R_g^2\rangle^{1/2}$ of PS at Different Pressures**

| pressure, MPa | $K$, cm³mol/g² | $A_2$, cm³mol/g² | $\langle R_g^2\rangle^{1/2}$, Å |
|---|---|---|---|
| 0 | 34.72 | 0.000 51 | 95.5 |
| 0.6 | 22.00 | 0.000 48 | 92.8 |
| 1.5 | 17.85 | 0.000 44 | 89.0 |
| 2.4 | 15.36 | 0.000 38 | 86.3 |
| 3.3 | 13.35 | 0.000 34 | 78.4 |
| 4.2 | 11.97 | 0.000 30 | 71.3 |

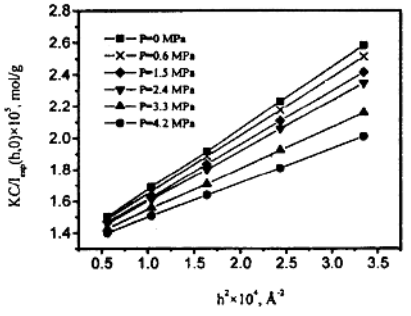


**Figure 11.** Plots of $KCI_{exp}(h,0)$ against $h^2$ for PS in toluene at different antisolvent $CO_2$ pressures.

$CO_2$. $A_2$ decreases with increasing antisolvent pressure, which indicates that the solvent power of toluene to PS decreases with adding of antisolvent $CO_2$.

To calculate the mean square radius of gyration $\langle R_g^2\rangle^{1/2}$ using eq 5, the data for $(KCI_{exp}(h,C))_{C=0}$ are required. To do this, $KCI_{exp}(h,C)$ is plotted against $C$. The values of $K$ in Table 2 were used in the calculation of $KCI_{exp}(h,C)$. $KCI_{exp}(h,C)$ vs $C$ curves were extrapolated to zero concentration, and $(KCI_{exp}(h,C))_{C=0}$ was obtained. $(KCI_{exp}(h,C))_{C=0}$ vs $h^2$ curves are linear, as shown in Figure 11. Thus, $\langle R_g^2\rangle^{1/2}$ can be evaluated from their slopes as can be known from eq 5. The results are given in Table 2 and Figure 12. The $\langle R_g^2\rangle^{1/2}$ of PS in toluene ($CO_2$-free) agrees with the literature value (97.7 Å).[51]

As shown in Figure 12, $\langle R_g^2\rangle^{1/2}$ decreases with increasing pressure. It indicates that the PS chain experiences shrinking in the course of adding antisolvent $CO_2$. Toluene is a good solvent for PS, and the coil expanded due to prevailing intersegmental repulsion; after addtion of $CO_2$, the solvent power of the solvent is reduced and PS chain is shrunk due to prevailing intersegmental attraction. This conclusion is the same as that obtained from the dependence of intrinsic viscosity on pressure.

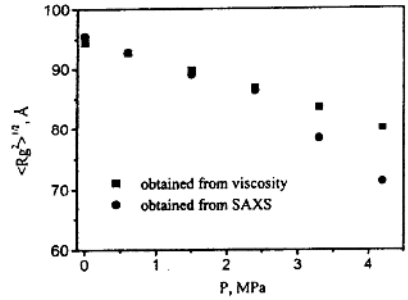


**Figure 12.** Effect of antisolvent $CO_2$ pressure on the $\langle R_g^2\rangle^{1/2}$ at 308.15 K

As discussed above, $[\eta]$ is related with $\langle R_g^2\rangle^{1/2}$ by eq 1.[31] The $\langle R_g^2\rangle^{1/2}$ values, calculated from eq 1 and $[\eta]$ obtained in this work, are also shown in Figure 12. We can see that the values of $\langle R_g^2\rangle^{1/2}$ obtained from viscosity data agree reasonably with those from SAXS method, especially at the lower $CO_2$ pressures. This implies that Flory theory, which has been used widely for the solutions of polymers in liquid solvents, is also applicable to the polymer solution with gas antisolvent.

**Acknowledgment.** This work was supported by the National Basic Research Project-Macromolecular Condensed State and the National Natural Science Foundation of China(29633020, 29725308). The authors are also grateful to Dr. R. K. Thomas for his advice.

## References and Notes

(1) McHugh, M. A.; Krukonis, V. J. *Supercritical Fluids Extraction Principles and Practice*, 2nd ed.; Butterworth-Heinemann: Stoneham, MA, 1994; p 189.
(2) Li, D.; Han, B. X. *Macromolecules* **2000**, *33*, 4555.
(3) Arora, K. A.; Lesser, A. J.; McCarthy, T. J. *Macromolecules* **1999**, *32*, 2562.
(4) Shiho, H.; Desimone, J. M. *J. Polym. Sci., Part A: Polym. Chem.* **1999**, *37*, 2429.
(5) Mishima, K.; Matsuyama, K.; Tanabe, D.; Yamauchi, S.; Young, T. J.; Johnston, K. P. *AIChE J.* **2000**, *46*, 857.
(6) Eckert, C. A.; Knutson, B. L.; Debenedetti, P. G. *Nature* **1996**, *383*, 313.
(7) Dixon, D. J.; Johnston, K. P.; Bodmeier, R. A. *AIChE, J.* **1993**, *39*, 127.
(8) Gallagher, P. M.; Coffey, M. P.; Krukonis, V. J. *J. Supercrit. Fluids* **1992**, *5*, 130.
(9) Robertson, J.; King, M. B.; Swcille, J. P. K.; Merrifield, D. R.; Buxton, P. C. *Proceedings of the 4th International Symposium on Supercritical Fluids*; 1997; p 47.
(10) Shishikura, A. *Proceedings of the 4th International Symposium on Supercritical Fluids*; 1997, p 51.
(11) Catchpole, O. J.; Hochmann, S.; Anderson, S. R. J. In *High-Pressure Chemical Engineering*; Rudolf von Rohr, P., Trepp, C., Eds.; 1996; p 309.
(12) Reverchon, E.; Della Porta, G.; Trolio Di, A.; Pace, S. *Ind. Eng. Chem. Res.* **1998**, *37*, 952.
(13) Reverchon, E.; Della Porta, G.; Sannino, D.; Ciambelli, P. *Powder Technol.* **1999**, *102*, 127.
(14) Reverchon, E. *J. Supercrit. Fluids* **1999**, *15*, 1.
(15) Dixon, D. J.; Johnston, K. P. *J. Appl. Polym. Sci.* **1993**, *50*, 1929.
(16) Lele, A.; Shine, A. D. *AIChE J.* **1992**, *38*, 742.
(17) Mawson, S.; Johnston, K. P.; Betts, D. E.; McClain, J. B.; DeSimone, J. M. *Macromolecules* **1997**, *30*, 71.
(18) Luna-Barcenas, G.; Kanakia, S. K.; Sanchez, I. C.; Johnston, K. P. *Polymer* **1995**, *36*, 3173.

(19) Yeo, S.-D.; Debenedetti, P. G.; Radosz, M.; Giesa, R.; Schmidt, H.-W. *Macromolecules* **1995**, *28*, 1316.
(20) Yeo, S.-D.; Debenedetti, P. G.; Radosz, M.; Schmidt, H.-W. *Macromolecules* **1993**, *26*, 6207.
(21) Dixon, D. J.; Luna-Barcenas, G.; Johnston, K. P. *Polymer* **1994**, *35*, 3998.
(22) Luna-Barcenas, G.; Kanakia, S. K.; Sanchez, I. C.; Johnston, K. P. *Polymer* **1995**, *36*, 3173.
(23) Tuminello, W.; Dee, G. T.; McHugh, M. A. *Macromolecules* **1995**, *28*, 1506.
(24) Glatter, O.; Kartky, O. *Small-Angle X-ray Scattering*; Academic Press: New York, 1982.
(25) McClain, J. B.; Londino, D.; Combes, J. R.; Romack, T. J.; Canelas, D. A.; Betts, D. E.; Wignall, G. D.; Samulski, E. T.; DeSimone, J. M. *J. Am. Chem. Soc.* **1996**, *118*, 917.
(26) Hayashi, H.; Hamada, F.; Nakajima, A. *Macromolecules* **1974**, *7*, 959.
(27) Fujiwara, Y.; Flory, P. J. *Macromolecules* **1970**, *3*, 288.
(28) Yoon, D. Y.; Flory, P. J. *Macromolecules* **1976**, *9*, 294.
(29) Hyman, A. S. *Macromolecules* **1975**, *8*, 849.
(30) Smith, T.; Carpenter, D. K. *Macromolecules* **1968**, *1*, 204.
(31) Flory, P. *Principles of polymer chemistry*; Cornell University Press: Ithaca, NY, 1953.
(32) Wolf, B. A.; Jend, R. *Macromolecules* **1979**, *12*, 732.
(33) Geerissen, H.; Schmidt, J. R.; Wolf, B. A. *J. Appl. Polym. Sci.* **1982**, *27*, 1277.
(34) Kiran, E.; Zhuang, W. H. *Polymer* **1992**, *33*, 5259.
(35) Mertsch, R.; Wolf, B. A. *Macromolecules* **1994**, *27*, 3289.
(36) Terao, K.; Hokajo, T.; Nakamura, Y.; Norisuye, T. *Macromolecules* **1999**, *32*, 3690.
(37) Kubota, K.; Ogina, K. *Macromolecules* **1979**, *12*, 74.
(38) Schmidt, J. R.; Wolf, B. A. *Macromolecules* **1982**, *15*, 1192.
(39) Schott, N.; Will, B.; Wolf, B. A. *Makromol. Chem.* **1988**, *189*, 2067.
(40) Geerissen, H.; Gernandt, F.; Wolf, B. A. *Makromol. Chem.* **1991**, *192*, 165.
(41) Gaeckle, D.; Patterson, D. *Macromolecules* **1972**, *5*, 136.
(42) Li, D.; Liu, Z. M.; Yang, G. Y.; Han, B. X.; Yan, H. K. *Polymer* **2000**, *41*, 5707.
(43) Han, B. X.; Ke, J.; Yan, H. K.; Bo, Z. Y.; Zhang, S. Z. Chinese Patent No. 94215865.2.
(44) Han, B. X.; Peng, D. Y.; Fu, C. T. *Can. J. Chem. Eng.* **1992**, *70*, 1164.
(45) Lu, J.; Han, B. X.; Yan, H. K. *Phys. Chem. Chem. Phys.* **1999**, *1*, 449.
(46) Dong, B. Z.; Sheng, W. J.; Yang, H. L.; Zhang, Z. J. *J. Appl. Crystallogr.* **1997**, *30*, 877.
(47) Huggins, M. L. *J. Am. Chem. Soc.* **1942**, *64*, 2716.
(48) Des cloizeaux, J. *J. Phys.* **1975**, *36*, 281.
(49) De gennes, P. G. *Macromolecules* **1976**, *9*, 587.
(50) Desjardins, A.; Van de Ven, T. G. M.; Eisenberg, A. *Macromolecules* **1992**, *25*, 2412.
(51) Berry, G. C. *J. Chem. Phys.* **1966**, *44*, 4550.

MA0014463

Chinese Chemical Letters Vol. 12, No. 8, pp 741 – 744, 2001 

# Determination of Average Wall Thickness of Mesoporous Silica

Zhi Hong LI[1], Yan Jun GONG[1], Dong WU[1], Yu Han SUN[1]*, Jun WANG[2], Yi LIU[2], Bao Zhong DONG[2]

[1]State Key Laboratory of Coal Conversion, Institute of Coal Chemistry, Chinese Academy of Sciences, P.O.Box 165,Taiyuan 030001

[2]Laboratory of Synchrotron Radiation, Institute of High Energy Physics, Chinese Academy of Sciences, P.O.Box 918, Beijing 100039

**Abstract:** Small Angle X-ray Scattering (SAXS) experiment using Synchrotron Radiation as X-ray source was used to determine the average wall thickness of mesoporous silica prepared by condensation of tetraethylorthosilicate (TEOS) using non-ionic alkylpolyethyleneoxide ($AEO_9$) surfactant as templates. The results agreed with that of high-resolution TEM (HRTEM) measurement.

**Keywords:** Small Angle X-ray Scattering (SAXS), mesoporous silica, average wall thickness.

Mesoporous silica formed by the condensation of silica oligomers around self-assembled surfactant micelle templates has recently attracted much interest owing to its potential for use in catalytic or adsorbent applications[1]. Much attention has been focused on characterization of its pore structure by transmission electron microscopy (TEM), high-resolution TEM (HRTEM), $N_2$ adsorption, small angle X-ray scattering (SAXS) *et al.*, but seldom concerning its average wall thickness[2-7]. This short communication introduced a flexible method to evaluate the average wall thickness of mesoporous silica under examination by SAXS.

Mesoporous silica was prepared using tetraethylorthosilicate (TEOS) as precursor and non-ionic alkylpolyethyleneoxide $CH_3(CH_2)_n(OCH_2CH_2)_9OH$ ($AEO_9$) surfactant as templates[8]. The surfactant extraction was performed by Soxhlet extraction with ethanol for 24h, and then the final solid was filtered, washed with distilled water and dried at 100°C in air.

XRD measurement indicated that the resultant silica was in amorphous state. $N_2$ adsorption at −196°C with ASAP2000 and HRTEM measurement (see **Figure 1**) with HITACHI-9000 illustrated that the sample was of mesoporous structure.

SAXS experiment was performed using Synchrotron Radiation as X-ray source with a long-slit collimation system at Beijing Synchrotron Radiation Laboratory. Incident X-ray wavelength $\lambda$ was 0.154nm, and the scattering angle $2\theta$ was approximately 0~3°, the scattering vector was denoted as $q$, where $q=4\pi\sin\theta/\lambda$. The scattered X-ray intensity was recorded using imaging plate technology. The

background scattering and the absorption of the sample were corrected. Data analysis was directly based on slit-smeared intensity $J(q)$.

Figure 1 HRTEM image of a representative region of mesoporous silica

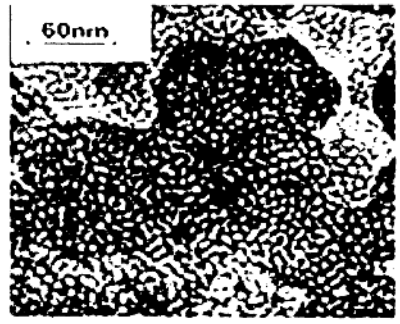


In the small angle X-ray scattering of ideal two-phase system of mesoporous material, there is the following relation between the average pore size $l_p$, the average wall thickness of the solid matrix $l_s$ and the correlation distance $a_c$ that is a measure of phase size[9]:

$$\frac{1}{a_c} = \frac{1}{l_p} + \frac{1}{l_s} \qquad (1)$$

Thus, once $a_c$ and $l_p$ have been determined, $l_s$ could then be deduced from the formula (1). In this paper, $a_c$ and $l_p$ were determined from Debye plot and Guinier plot, respectively.

Guinier plot of the sample (see **Figure 2**) is continuous and strongly concave shows that the pores, which give the small angle X-ray scattering[10], in the sample are polydispersive[10]. The relation between the scattering intensity $J(q)$ and the pore size distribution $V_i(D)$~$D_i$ is as following[11]:

Figure 2 ln[J (q)] *versus* $q^2$ plot of mesoporous silica

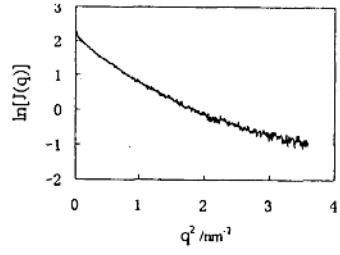

$$J(q) = \sum_{i=1}^{n} CV_i D_i^3 \exp(-\frac{3}{20} D_i^2 q^2) \quad (2)$$

where C is a constant, $V_i(D)$ is the fraction of the volume of the pores with diameter $D_i$ to the total volume of all pores in the sample. By using the Shull-Roess method[12], the pore size distribution $V_i(D)$~$D_i$ is deduced from equation (2) and **Figure 2**[13]. The average pore diameter $l_p$ can then be determined as:

$$l_p = \sum_{i=1}^{n} D_i V_i \quad (3)$$

The result is that $l_p$ equals to 2.86nm.

**Figure 3** is Debye plot of the sample. The well linear relation in **Figure 3** indicates that the sample is a completely random two-phase system, *i.e.* the uniform electron density of certain value in the silicon matrix and the zero electron density in pores. According to Debye's theory[14], for slit-smeared intensities[15]:

**Figure 3** $J(q)^{-2/3}$ *versus* $q^2$ plot of mesoporous silica

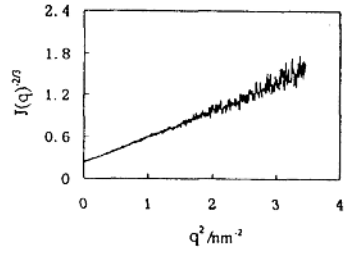


$$J(q) = \frac{A}{(1 + a_c^2 q^2)^{3/2}} \quad (4)$$

where $A$ is a constant. Thence $a_c$ may be evaluated from **Figure 3**, where

$$a_c = \left( \frac{Slope}{Intercept} \right)^{1/2} \quad (5)$$

The result is that $a_c$ equals to 1.18nm.

Having obtained $a_c$ and $l_p$, the average wall thickness $l_s$ in the sample could then be determined with formula (1), and the result is that $l_s$ equals to 2.01nm. This lies within the range of 1.50nm to 3.50nm obtained from HRTEM experiment in **Figure 1**.

Unlike other characterizing techniques such as gas adsorption, TEM and HRTEM, SAXS can be used to the study of the microstructure of both wet and dry porous materials whether the pores are open or closed. So, comparatively speaking, measurement of the average wall thickness of mesoporous material by SAXS represents probably the value close to the absolute limit.

**Acknowledgments**

This work was supported by the National Natural Science Foundation of China (Grant No.29625307 and No.29973057) and the National Key Basic Research Special Foundation (G20000480).

**References**

1. J. Edler, J W. White, *J. Mater. Chem.*, **1999**, *9*, 2611.
2. Z. H. Li, J. H. Sun, J. P. Zhao, D. Wu, Y. H. Sun Yuhan, *Acta Physica Sinica*, **2000**, *49* (7), 1312 (in Chinese).
3. P. W. J. G. Wijnen, T. P. M. Beelen, K. P. J. Rummens, H. C. P. L. Saeijs, R. A. V. Santen, J. *Appl. Cryst.*, **1991**, *24*, 759.
4. N. A. Clark, T. Bellini, R. M. Malzbender, B. N. Thomas, *et. al.*, *J. Appl. Cryst.*, **1993**, *71*, 3505.
5. P. Fratzl, G. Vogl,. S. Klaumunzer, J. Appl. Cryst., **1991**, *24*, 588.
6. P. W. Schmidt, J. Appl. Cryst., **1991**, *24*, 414.
7. T. R. Pauly, Y. Liu, T. J. Pinnavaia, S. J. L. Billinege, T. P. Rieker, *J. Am. Chem. Soc.*, **1999**, *124*, 8835.
8. Y. J. Gong, Y. Li, S. G. Wang, D. Wu, Y. H. Sun, *Chemical Journal of Chinese Universities*, **2000**, *21*, 1916.
9. G. W. Pei, W. L. Zhong, S. B. Yue, *X-ray Diffraction of Monocrystal, Polycrystal and Noncrystal Matter*, Shangdong University Press, Jinan, **1989**, pp.386-445 (in Chinese).
10. M. Setek, H. K. Wagenfeld, W. O. Stacy, L. T. Kiss, *Fuel*, **1983**, *62*, 480.
11. C. L. Guo, Y. H. Huang, *J. Inorganic Mater.*, 1991, *6* (3), 336 (in Chinese).
12. Z. F. Meng, *Theory and Application of Small Angle X-ray Scattering*, Jinlin Science and Technology Press, Changchun, **1996**, pp.29-30 (in Chinese).
13. S. T. Huang, *Structure and Structural Analysis of Noncrystal Material*, Science and Technology Press, Beijing, **1987**, p.142 (in Chinese).
14. P. Debye, A. M. Bueche, *J. Appl. Phys.*, **1949**, *20*, 518.
15. D. S. Brown, F. P. Warner, R. E. Wetton, *Polymer*, **1972**, *13* (12), 575.

Received 31 January, 2001

Vol 10 No 5, May 2001
1009-1963/2001/10(05)/0429-04

Chinese Physics



# STUDY OF MESOPOROUS SILICA MATERIALS BY SMALL ANGLE X-RAY SCATTERING*

LI ZHI-HONG(李志宏)[a], GONG YAN-JUN(巩雁军)[a], ZHANG YE(张 晔)[a], WU DONG(吴 东)[a], SUN YU-HAN(孙予罕)[a]†, WANG JUN(王 俊)[b], LIU YI(柳 义)[b], and DONG BAO-ZHONG(董宝中)[b]

[a] *State Key Laboratory of Coal Conversion, Institute of Coal Chemistry, Chinese Academy of Sciences, Taiyuan* 030001, *China*

[b] *National Synchrotron Radiation Laboratory, Institute of High Energy Physics, Chinese Academy of Sciences, Beijing* 100039, *China*

(Received 1 November 2000; revised manuscript received 15 January 2001)

Small angle X-ray scattering experiments have been performed to study the microstructure of mesoporous silica materials prepared by condensation of tetraethylorthosilicate using non-ionic alkylpolyethyleneoxide ($AEO_9$) and ionic cetyltrimethylammonium bromide (CTAB) surfactant as templates. It is the pores within the nanometre range that produce the main scattering. The scattering of the pure silica systems obey Porod's law. The scattering of the systems with templates remaining in the pores show positive deviations from Porod's law. This may be because the templates produce some additional scattering background and then make the scattering of pores distorted. The results show that the full removal of templates from the pores of the materials by Soxhlet extraction is very easy for $AEO_9$, but it is difficult for CTAB. The positive deviation correction is also performed.

**Keywords:** mesoporous silica, templates, small angle X-ray scattering
**PACC:** 6110, 6140

## I. INTRODUCTION

Mesoporous silica materials formed by the condensation of silica oligomers around self-assembled surfactant micelle templates have recently attracted much interest owing to their potential for use in catalytic or adsorbent applications.[1-3] Structural characterization of these materials is therefore of fundamental importance. Commonly, the pore structure of porous silica is measured by gas adsorption and transmission electron microscopy (TEM), but these techniques cannot 'see' the closed pores and the pores filled with a certain medium such as templates. Small angle X-ray scattering (SAXS) does not suffer from this restriction, since it arises from spatial fluctuations of the electronic density within the material. Thus, SAXS has been used in the study of porous silica materials.[3,4] Unfortunately, no information concerning the scattering by templates within the materials has been found. In fact, templates might exert some influence on the physical and chemical properties of the materials, though the influence and the acting mechanism remain equivocal until now. Therefore, this paper mainly aims at an understanding of the scattering phenomena caused by the templates in porous materials and the corresponding structural characteristics of mesoporous silica materials with or without templates, respectively.

## II. EXPERIMENTAL DETAILS

Mesoporous silica were prepared by an improved synthesis strategy using tetraethoxysilane (TEOS) as precursor and non-ionic alkylpolyethyleneoxide $CH_3(CH_2)_n(OCH_2CH_2)_9OH$ ($AEO_9$) or cetyltrimethylammonium bromide $C_{16}H_{33}N(CH_3)_3Br$ (CTAB) surfactant as templates.[5] The surfactant extractions were performed by Soxhlet extraction with ethanol for 24h, and then the final solids were filtered, washed with distilled water and dried at 100°C in air. Some samples were calcined at 550°C at heating rate of 1°C/min. The resultants are listed in Table 1, where the template/silica molar ratios for all samples are the same.

*Project supported by the National Natural Science Foundation of China (Grant Nos.29625307 and 29973057), and the National Key Basic Research Special Foundation of China (G20000480).

†Corresponding author, Fax:(0351)4041153; E-mail:yhsun@sxicc.ac.cn

**Table 1.** SAXS results of the mesoporous silica.

| Sample | Template | Extraction | Calcination temperature/°C | Slope of $\ln[q^3J(q)]$ vs. $q^2$ in high angle range | Average pore radius of gyration/nm |
|---|---|---|---|---|---|
| GZ1 | $AEO_9$ | No | | +0.257 | 1.79 |
| GZ2 | $AEO_9$ | Yes | | 0 | 1.65 |
| GZ3 | $AEO_9$ | No | 550 | 0 | 1.64 |
| GZ4 | CTAB | No | | +1.872 | 2.01 |
| GZ5 | CTAB | Yes | | +0.805 | 1.50 |
| GZ6 | CTAB | No | 550 | 0 | 1.32 |

SAXS experiments were performed using synchrotron radiation as an X-ray source with a long-slit collimation system at the Beijing Synchrotron Radiation Facility. The incident X-ray wavelength $\lambda$ was 0.154nm, and the scattering angle $2\theta$ was approximately 0°–3°, the scattering vector was denoted as $q$, $q=4\pi\sin\theta/\lambda$. The scattered X-ray intensities were recorded using imaging plate technology. The air scattering and the absorption of the sample were corrected.

## III. RESULTS AND DISCUSSION

X-ray diffraction (XRD) measurements have indicated that all samples in Table 1 are in the amorphous state. $N_2$ adsorption at 77K with ASAP2000 and high-resolution TEM (HRTEM) measurements have illustrated that all the samples are of mesoporous structure.

SAXS data analysis was directly based on slit-smeared intensities $J(q)$. A Porod plot (see Fig.1), i.e. $\ln[q^3J(q)]$-$q^2$ curve,[6–8] is used to determine whether the scattering system is ideal or not. The results are given in Table 1. The average pore radii of gyration obtained with SAXS (after correction of deviations from Porod's law) also show that the pores are nanometre-sized (see Table 1), which give rise to the SAXS.

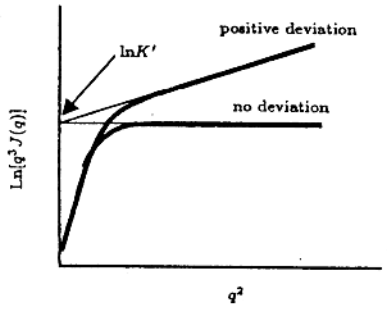


**Fig.1.** Porod plots and deviation correction.

It is very interesting that two types of Porod curves appear, i.e. no deviation and positive deviation from Porod's law (see Fig.2). This suggests that structural differences exist between these materials.

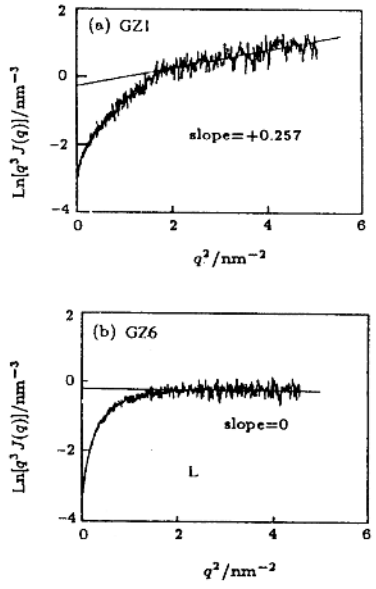


**Fig.2.** Porod plots of mesoporous silica.

According to Porod's law, for an ideal two-phase structure having sharply defined phase boundaries, the asymptotic behaviour of the intensity curve was found to be[9]

$$\lim J(q) = K'/q^3, \tag{1}$$

where $K'$ is a Porod constant. Formula (1) means that the slope of the $\ln[q^3J(q)]$-$q^2$ curve in the high $q$ range is close to zero. The slopes of $\ln[q^3J(q)]$-$q^2$ curves in the high-angle range of samples GZ2, GZ3 and GZ6